PHYSICAL REVIEW B VOLUME 35, NUMBER 15 15 MAY 1987-II

Interpretation of experiments implying density of states between Landau levels of a two-dimensional electron gas by a statistical model for inhomogeneities

Vidar Gudmundsson and Rolf R. Gerhardts
Max-Planck-Institut für Festkörperforschung, Heisenbergstrasse 1, Postfach 80 06 65, D-7000 Stuttgart 80, Federal Republic of Germany
(Received 15 September 1986)

A statistical model is presented for a spatially inhomogeneous two-dimensional electron gas in a quantizing magnetic field, which simulates the effect of Poisson's equation and some essential properties of self-consistent screening. The model yields an effective background density of states between Landau levels and is used to explain a number of recent experimental observations. A three-dimensional model of a heterojunction is introduced, which can account for the possible charge transfer between the gate and the two-dimensional electron gas. We show that for GaAs heterostructures the variation of the depletion length as a function of the magnetic field may be neglected.

I. INTRODUCTION

Recently measurements of the capacitance,[1,2] the activation energy,[3-5] the gate current,[1] the specific heat,[6] and the magnetization[7] of a two-dimensional electron gas (2D EG), in a strong quantizing magnetic field, have given strong indications for a considerable amount of density of states (DOS) in between the Landau levels (LL's). The effect is seen both in GaAs-(Ga,Al)As heterostructures and Si metal-oxide-semiconductor field-effect transistors (MOSFET's). The experimental results could be reproduced by model calculations, based on the *ad hoc* assumption that the DOS consists of broadened Gaussian shaped LL's superimposed on a constant, magnetic-field-independent background DOS.[1,6]

Conventional perturbation theory of the interaction of the 2D EG with short-range impurities[8,9] and also recent exact theories of electrons in a random potential[10,11] predict that the DOS between the LL's should be vanishingly small in the large magnetic field regime. Thus, the occurrence of a finite background DOS between the LL's is unexpected and requires explanation.

A mechanism which might be capable of producing a considerable DOS between the LL's is scattering by long-range Coulomb potentials, e.g., of the donors which provide the electrons for the 2D EG in a heterostructure. Since screening is the more effective the higher the DOS, the level broadening depends on the position of the Fermi energy and oscillates as a function of the magnetic field, i.e., of the filling of the LL Such oscillations of the linewidth of the LL's have indeed been observed recently in cyclotron resonance experiments.[12] Recent self-consistent screening theories[13-15] indicate that, if the Fermi energy is located between two LL's, the level broadening may become so large that adjacent LL's overlap considerably even in the large magnetic field regime.[14,15] In this situation the predictions of these theories are, however, not reliable since they are based on assumptions (neglect of coherent multiple scattering processes and decoupled LL's), which lead to a semielliptical shape for the DOS of an individual LL and a break down for overlapping LL's.

It has also been emphasized that spatial inhomogeneities in the electron density, which are known to be present in all the investigated samples, can increase the effective broadening of the LL's.[1,2,16] In a recent publication[17] we discussed a statistical model for inhomogeneities which can produce an effective DOS between the LL's, and can also simulate qualitatively some characteristic features of the self-consistent screening mechanism. In the present paper we apply this statistical model to the calculation of measurable quantities and we will find that it can explain the experimental results at least as well as the *ad hoc* model of a constant background DOS.

Some of the measurable quantities, e.g., capacitance and specific heat, can be discussed within a strictly two-dimensional model with constant electron density, and the statistical model developed previously[17] can immediately be applied. Others, e.g., the recharging current which flows between the 2D EG and the gate while sweeping the magnetic field and, thereby, changing the capacitance, are better discussed within the three-dimensional (3D) model of the inversion layer. In order to give a coherent description, we start in Sec. II with the three-dimensional treatment and reduce it, where possible, to the two-dimensional model. In the Appendix we show, for instance, that the magnetic-field dependence of the depletion charges is of no importance for the GaAs system. In Sec. III we discuss several interesting properties of the statistical model, e.g., the interrelation of its three-dimensional and its two-dimensional versions. Finally, in Sec. IV we compare the results of the statistical model with experiments and other model calculations.

II. 3D MODEL OF THE HETEROSTRUCTURE

The electrical subband structure has been calculated by several authors both for Si-MOSFET's (Refs. 18 and 19) and GaAs heterostructures.[20-22] In this paper the simple self-consistent variational method of Fang and Howard[18]

 ©1987 The American Physical Society

within the Hartree approximation will be used for heterostructures that may have a gate. The effect of a variable depletion layer thickness together with the question whether the 2D EG is in equilibrium with the bulk will be considered. In order to compare results with the gate-current measurements[1] we will also discuss the case of variable electron density n_s due to an external circuit between the 2D EG and the gate. Initially the sample will be assumed to be homogeneous in the directions parallel to the insulator-semiconductor interface. In order to determine the electrical subband structure the Schrödinger and the Poisson equations for the electrons and the immobile charges in the heterostructure have to be solved self-consistently. The external magnetic field **B** perpendicular to the interface will lead to the familiar LL splitting of the subbands. The heterostructure is shown schematically in Fig. 1. The coupled equations for the subband envelope functions $\chi_i(z)$ and the charges $\rho(z)$ in the effective-mass approximation are then

$$\left[-\partial_z \frac{\hbar^2}{2m}\partial_z + V(z)\right]\chi_i(z) = E_i\chi_i(z) , \tag{2.1}$$

$$\partial_z K \partial_z \phi(z) = -4\pi\rho(z) , \tag{2.2}$$

with

$$V(z) = -e\phi(z) + \Delta V_c(z) , \tag{2.3}$$

$$\rho(z) = \rho_{im}(z) - e\sum_i [\chi_i(z)]^2 n_i . \tag{2.4}$$

Here $\rho_{im}(z)$ represents the gate charges and assumed uniform acceptor and donor charges in the semiconductor and the insulator, respectively. K stands for the (slightly different) dielectric constants of these two materials and m for their effective masses. n_i ($n_s = n_0$) is the areal electronic density of the ith band while $\Delta V_c(z)$ is the conduction-band edge at the interface. Numerical solutions of (2.1)–(2.4) by Stern and Das Sarma[23] and variational solution by Bastard[24] have shown that the neglect of the penetration of the electrons into the insulator introduces only a small error to the results. We will therefore assume that the electrons are confined to the semiconductor and in order to obtain analytical results, to simplify the later introduction of statistical inhomogeneities in n_s, we adapt the ansatz for the wave function,

$$\chi_0(z) = \left[\frac{b^3}{2}\right]^{1/2} z e^{-bz/2} , \tag{2.5}$$

where b is a variational parameter to be fixed by the self-consistency requirement, and the origin is assumed to be at the interface. In accordance with experimental evidence at very low temperature T for the equilibrium properties we are interested in, only the lowest subband will be assumed occupied and all the donors in the insulator are considered ionized.

We consider two models for the inversion layer. In the first the 2D EG is in equilibrium with the electrons of the bulk semiconductor, and the depletion length d is calculated self-consistently for a given homogeneous acceptor concentration.

In addition to the total charge neutrality of the heterostructure we require

$$-e\phi(d) = E_F + E_G - E_A , \tag{2.6}$$

where E_F is the Fermi energy level, E_G is the band gap of

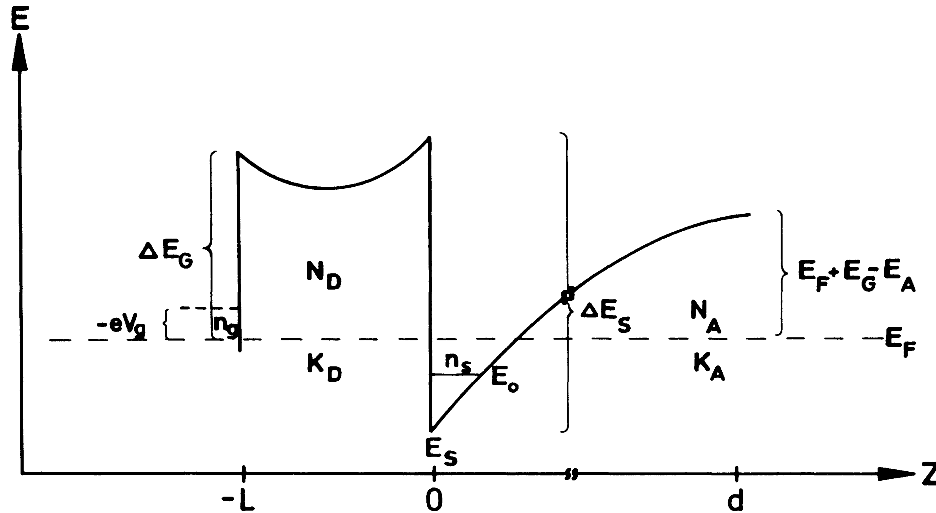

FIG. 1. A schematic figure of a heterostructure, where E_F is the Fermi level; E_0 is the lowest electrical subband; E_s is the bottom of the confining potential; n_s is the density of 2D EG; N_A is the density of acceptors in the GaAs; N_D is the density of donors in the $Ga_{1-x}Al_xAs$; K_D is the dielectric constant of the insulator; K_A is the dielectric constant of the semiconductor; ΔE_s is the conduction-band offset; ΔE_G is the Schottky barrier; en_g is the gate charge density; V_g is the gate voltage; E_G is the energy gap of the semiconductor; and E_A is the acceptor energy.

the semiconductor, and E_A is the acceptor energy, i.e., the Fermi level is fixed at the acceptor energy in the bulk semiconductor. The charge neutrality is then reflected in the condition that the electric field $-\phi'(z)$ vanishes as $z \to \pm\infty$. The calculations for this model are performed in the Appendix where we see that for GaAs heterostructures the variation of n_s and $N_A d$ is insignificant and can be neglected. This is due to the large depletion length of GaAs heterostructures. The $N_A d$ variation may, however, be important in materials with short d as, for example, $In_xGa_{1-x}As_yP_{1-y}/InP$ (Ref. 25) and may in such cases modify the measured capacitance significantly as is shown in the Appendix. In the second model the 2D EG is not in equilibrium with the bulk semiconductor and the depletion charge $N_A d$ will be considered constant. In this case the electrical field at the interface $-\phi'(0) = V'(0)/e$ will be specified. This model will still be able to account for a charge transfer via an external circuit between the 2D EG and a possible gate on the heterostructure, as is needed to explain the gate-current and the capacitance measurements, and we will discuss only this model in the following.

The self-consistency requirement for solving (2.1)—(2.4) with the variational ansatz (2.5) is now fulfilled in the following way. First the Poisson equation (2.2) is solved together with the ansatz (2.5) giving the potential $V(z,b)$, where b is the still-free variational parameter.

Next the variational ansatz (2.5), with a new parameter $\tilde{b}$, is used to evaluate $\langle E_{\text{kin}} + V(z,b) \rangle_{\tilde{b}}$ which is then minimized with respect to $\tilde{b}$ in order to derive the lowest subband energy $E_0(\tilde{b}_0, b)$. The self-consistency is then satisfied by assuming that the parameter b used in the first step is in reality the parameter $\tilde{b}_0$ determined from the minimization of the subband energy, i.e., $b \equiv \tilde{b}_0$. In evaluating the expectation value of the potential $\langle V(z) \rangle$ a term of the order of $(z/d)^2$ is neglected due to the small extent, $1/b$, of the wave function compared with the depletion layer thickness d (see the Appendix for details). The variational calculation yields a relation between n_s and $E_0 - E_s$, where E_s is the depth of the potential well at the interface $[E_s = V(0^+)]$. The chemical potential

$$\mu = E_F - E_0 , \tag{2.7}$$

is related to n_s by

$$n_s = \int_{-\infty}^{\infty} dE\, D(E) f(E-\mu) . \tag{2.8}$$

The gate voltage V_g can be expressed in terms of $E_F - E_s$, the conduction band offsets at the AlGaAs-barrier surfaces and the variation of the electrostatic potential across the barrier. Using the condition of charge neutrality,

$$n_g + N_D L = N_A d + n_s , \tag{2.9}$$

we obtain

$$eV_g = \mu - (E_s - E_0) + \frac{4\pi e^2 L}{K_D} n_g + K_1 . \tag{2.10}$$

Here $D(E)$ is the DOS, en_g the density of gate charges, L is the thickness of the insulator, K_1 is a constant depending on the band offset at the interface and the Schottky barrier, and N_D is the donor concentration. E_0 is the electric subband energy:

$$E_0 - E_s = \frac{4\pi e^2}{K_A} \frac{3}{b} \left(\tfrac{55}{64} n_s + \tfrac{3}{2} N_A d \right) \tag{2.11}$$

with

$$b = \left[\frac{33\pi}{2a_B} \left(n_s + \tfrac{32}{11} N_A d \right) \right]^{1/3} , \tag{2.12}$$

where $a_B = K_A \hbar^2 / me^2$ is the effective Bohr radius of the electrons of GaAs.

We will now distinguish two different cases of this model corresponding to different experimental setups. When the current between the 2D EG and the gate is measured as a function of B,[1] or when the capacitance is measured,[1,2] then the gate voltage V_g is essentially held constant while n_s can vary with B. In that respect we will consider the case when V_g and $N_A d$ is held constant. The differential capacitance per area can then be found by differentiating Eq. (2.10) with respect to n_s, using Eq. (2.11):

$$C = \frac{e\,dn_s}{dV_g} = \left[\frac{4\pi L}{K_D} + \frac{1}{e^2 D_T} + \frac{4\pi}{K_A b} \frac{55}{32} \left[\frac{1 + \dfrac{192}{55} \dfrac{N_A d}{n_s}}{1 + \dfrac{32}{11} \dfrac{N_A d}{n_s}} \right] \right]^{-1} , \tag{2.13}$$

where D_T is the thermodynamic density of states (TDOS):

$$D_T = \frac{dn_s}{d\mu} . \tag{2.14}$$

The gate current per area is

$$I_g = -e \left[\frac{dn_s}{dt} \right]_{V_g} = -e \left[\frac{\partial n_s}{\partial B} \right]_{\mu} \frac{C}{e^2 D_T} \frac{dB}{dt} . \tag{2.15}$$

On the other hand, the specific heat and the magnetization are measured in heterostructures without a gate, and n_s is kept constant. In this case we set no restriction on V_g but require n_s to be held fixed. (For convenience we set $N_A d = 0$ in this case.) We introduce the free energy F and the internal energy U per sample area:

$$F = n_s \mu - \frac{1}{\beta} \int_{-\infty}^{\infty} dE\, D(E) \ln(1 + e^{-\beta(E-\mu)}) , \tag{2.16}$$

$$U = \int_{-\infty}^{\infty} dE\, D(E) E f(E-\mu) , \tag{2.17}$$

where $\beta = 1/k_B T$. Then the specific heat C_v and the magnetization M can be evaluated:[26]

$$C_v = \left[\frac{\partial U}{\partial T} \right]_{B,V} , \tag{2.18}$$

$$M = -\left[\frac{\partial F}{\partial B} \right]_{n_s,T} = -\left[\frac{\partial F}{\partial B} \right]_{\mu,T} + \left[\frac{\partial n_s}{\partial B} \right]_{\mu,T} . \tag{2.19}$$

This model has also been used to evaluate the capacitance of a heterostructure.[1,2] The expression for C in that case is formally the same as the $N_A d \to 0$ limit of Eq. (2.13).

III. THE STATISTICAL MODEL

Models of the 2D EG in a strong magnetic field, used to interpret experimental results, commonly include only the broadening of the LL's caused by short-range impurity scattering.[1–7] While the real broadening of LL's observed in experiments is in general larger than the short-range scattering theories[8,9] predict, attempts have been made to account for the additional broadening by inhomogeneities in the electron density n_s.[1,2] The introduction of inhomogeneities in n_s may be a simplified method to account for the scattering of electrons with partially screened long-range charged impurities or their interaction with the spatial inhomogeneities in the donor and the acceptor distributions. In that case the statistical distributions of n_s and μ would have to be evaluated by solving self-consistently the Schrödinger and Poisson equations, not only for the direction perpendicular to the interface, but also in the 2D EG layer parallel to the interface.

This is a difficult task closely related to the theories of self-consistent screening for long-range impurities.[14] Here we will instead select simple forms of distributions and compare the results, for the measurable quantities, qualitatively with experimental results. It will also become evident that some forms of the statistical model indeed mimic to a great extent the properties of the more involved self-consistent screening theories. Since the Poisson equation is not used for the 2D EG in the directions along the interface, the statistical model introduced here considers an ensemble of independent homogeneous subregions rather than spatial fluctuations within one sample.

Owing to the relation (2.8), the chemical potential μ together with the electron density n_s will be a random variable. Their probability distributions will be related by[17]

$$P_\mu(\mu) = P_n(n_s(\mu)) \frac{dn_s}{d\mu} . \tag{3.1}$$

Thus for the model where n_s is held constant a simple convenient form of a distribution will be selected either for P_μ or P_n. While the specific form of a distribution is definitely sample dependent, qualitative properties of the statistical model may be expected to be independent of the chosen distribution to some extent. With this in mind we will discuss the cases when either P_n or P_μ is a Gaussian distribution. In addition, the Gaussian form of P_μ together with the specific form of $D(E)$ chosen below will allow for illustrative analytical calculations of some of the model properties. Since the Fermi level E_F is considered to be constant over the whole sample, the fluctuations in μ have to be understood as being caused by the randomness of the electrical subband energy owing to fluctuations of the electrostatic potential along the interface. On the other hand, for the model where n_s is a function of B we will require $n_{s0} = n_s(B=0)$ to be Gaussian distributed implying that $\mu_0 = \mu(B=0)$ is also Gaussian distributed due to the linear relation between these two variables at zero magnetic field. In this model the standard deviations $\Delta\mu$ and Δn_s will both in general be functions of B since the deviation of n_{s0} is fixed. To distinguish between these three possibilities the names μ-, n_s-, or n_{s0}-Gaussian model will be used. To demonstrate the properties of the statistical model quantitatively, in the following the single particle DOS $D(E)$ will be assumed to be of a Gaussian form, as predicted by higher-order short-range scattering theories:[8,9]

$$D(E) = \frac{1}{(2\pi)^{1/2}\Gamma} \frac{1}{\pi l^2} \sum_{n=0}^{\infty} \exp\left[-\frac{(E-E_n)^2}{2\Gamma^2} \right] , \tag{3.2}$$

where Γ and E_n are the magnetic-field-dependent broadening parameter and the energy spectrum, respectively. Here we will adopt the results of the self-consistent Born approximation[8] for Γ and select the electron mobility such that[1]

$$\Gamma(B) = 0.3\sqrt{B[\mathrm{T}]}\ \mathrm{meV} . \tag{3.3}$$

The energy spectrum chosen will be that of free spin degenerate electrons in a perpendicular magnetic field:

$$E_n(B) = \hbar\omega_c(n + \tfrac{1}{2}) , \tag{3.4}$$

where ω_c is the effective cyclotron energy for GaAs. The following parameters will also be used; $n_s = 2.25\times 10^{11}$ cm^{-2}, $N_A d = 1.44\times 10^{11}$ cm^{-2}, $T = 1.64$ K. It should be emphasized that the qualitative behavior of the statistical model is independent of these choices. In Figs. 2–6 we show the typical features of the three statistical models to

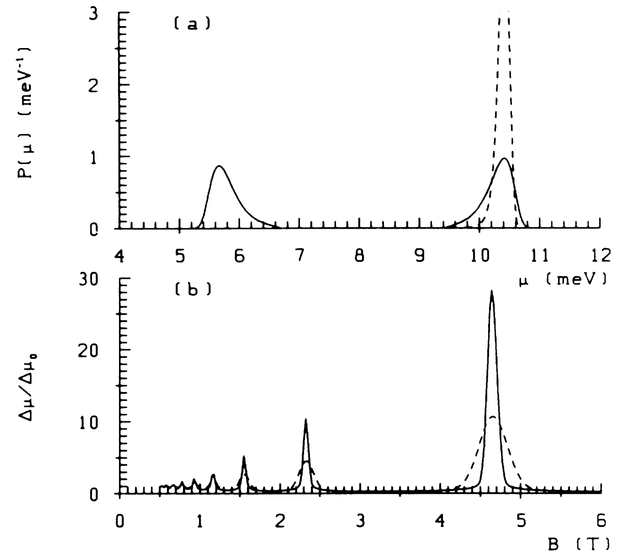

FIG. 2. (a) The probability distribution of the chemical potential μ of the n_s-Gaussian model with $\Delta n_s/\bar{n}_s = 0.01$ for $B=4.5$ T (dashed line) and $B=4.65$ T (solid line), $\bar{n}_s = 2.25\times 10^{11}$ cm^{-2}, $T=1.64$ K, and $\Gamma = 0.3\sqrt{B[T]}$ meV. For $B=4.5$ T the average $\langle\mu\rangle$ is inside a LL while for $B=4.65$ T it is well between two LL's. (b) The standard deviation of μ as a function of the magnetic field B for $\Delta n_s/\bar{n}_s = 0.01$ (solid line) and 0.03 (dashed line). $\Delta\mu_0$ is the standard deviation when $B=0.0$ T.

be discussed below. In Fig. 2(a) it is seen that the most probable value of the chemical potential $\langle\mu\rangle$ is strongly pinned to the LL's in the n_s-Gaussian model. As can be seen from Eq. (3.1) this is due to the fact that the TDOS is vanishingly small between LL's. As a consequence the average TDOS is finite even when $\langle\mu\rangle$ is in between LL's [cf. Fig. 6(a)], i.e., the effective thermodynamic DOS in an inhomogeneous sample is nonvanishing between the LL's. In a real inhomogeneous sample the strong pinning of μ to the LL's is hardly expected, since the potential variation between subregions pinned to different LL's is rather large, of the order $\hbar\omega_c$, while the variation inside each region must be smaller than $\Gamma \ll \hbar\omega_c$. The strong curvature of the potential therefore required at the boundaries between the subregions of the sample would be in conflict with the smoothness requirements of the Poisson equation.

For the Gaussian DOS $D(E)$ in Eq. (3.2) the μ-Gaussian model yields the analytical results:

$$\langle n_s\rangle = \int_{-\infty}^{\infty} dE\, D_{\mathrm{eff}}(E) f(E-\langle\mu\rangle) , \tag{3.5}$$

where $D_{\mathrm{eff}}(E)$ has the same form as the input DOS $D(E)$ [cf. Eq. (3.2)] with Γ replaced by Γ_{eff},

$$\Gamma_{\mathrm{eff}} = [\Gamma^2 + (\Delta\mu)^2]^{1/2} . \tag{3.6}$$

The TDOS does also have the simple form

$$\langle dn_s/d\mu\rangle = \partial\langle n_s\rangle / \partial\langle\mu\rangle .$$

As we have shown previously[17] the qualitative physical properties of the μ-Gaussian model are clearly illustrated using the simple approximation:

$$\Delta\mu \simeq \frac{\Delta n_s}{\langle dn_s/d\mu\rangle} . \tag{3.7}$$

Here it becomes clear that the assumption of a small but finite $\Delta\mu$ independent of B does not correctly simulate the behavior of a real sample. It would lead to vanishingly small Δn_s between LL's where the TDOS is small. One

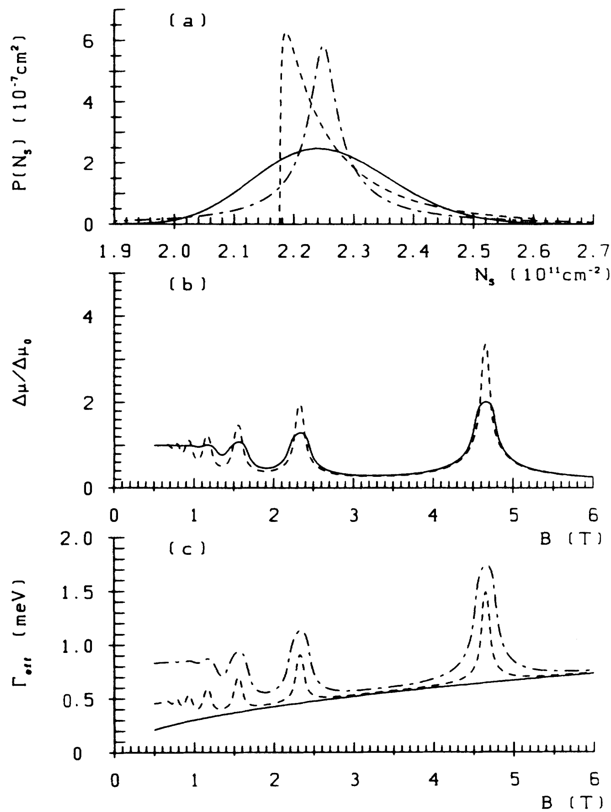

FIG. 3. (a) The probability distribution of the electron number density n_s of the μ-Gaussian model for $B=3.5$ T (solid line), 4.65 T (dashed-dotted line), and 4.5 T (dashed line) with $\Delta n_s/\bar{n}_s=0.05$. The parameters $\bar{n}_s$, T, and Γ are as in Fig. 1. (b) The standard deviation of μ as a function of B for $\Delta n_s/\bar{n}_s=0.1$ (solid line) and 0.05 (dashed line). $\Delta\mu_0$ is the standard deviation of μ when $B=0.0$ T. (c) The effective LL broadening vs B for $\Delta n_s/\bar{n}_s=0.0$ (solid line), 0.05 (dashed line), and 0.1 (dashed-dotted line).

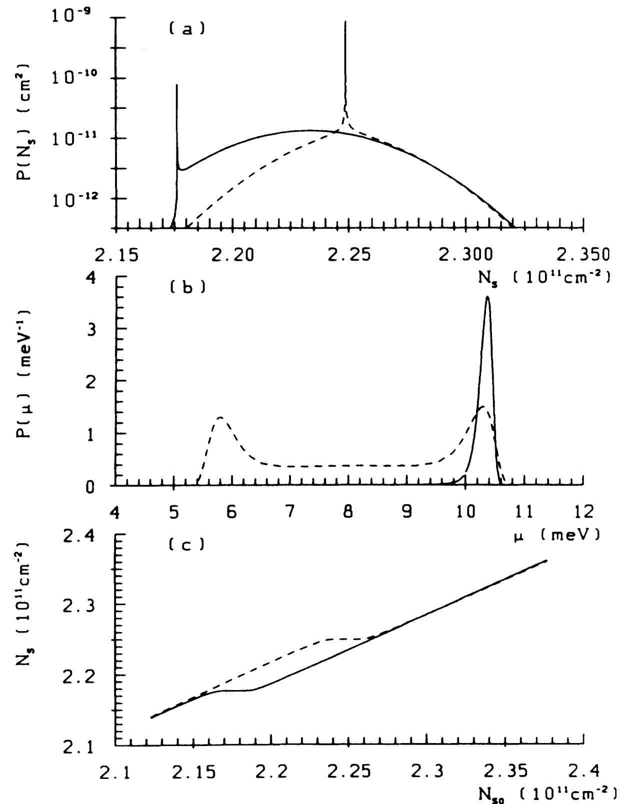

FIG. 4. The probability distribution of (a) the number density n_s and (b) the chemical potential for the n_{s0}-Gaussian model with $\Delta n_{s0}/\bar{n}_{s0}=0.01$ for $B=4.5$ T (solid line) and 4.65 T (dashed line) [dashed line shows $3P(\mu)$]. $\bar{n}_{s0}=2.25\times10^{11}$ cm^{-2}, $N_A d=1.44\times10^{11}$ cm^{-2}, and Γ and T as in Fig. 1. (c) The electron density $n_s(B)$ at $B=4.5$ T (solid line) and at 4.65 T (dashed line) as a function of the electron density n_{s0} at zero magnetic field.

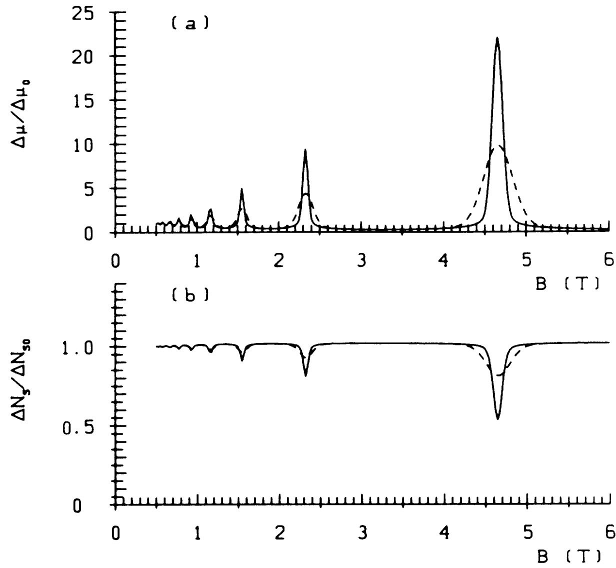

FIG. 5. (a) The standard deviation of the chemical potential $\Delta\mu$ as a function of B for the n_{s0}-Gaussian model with $\Delta n_{s0}/\bar{n}_{s0}=0.01$ (solid line) and 0.03 (dashed line). $\bar{n}_{s0}=2.25\times10^{11}$ cm^{-2}, $N_A d=1.44\times10^{11}$ cm^{-2}, and Γ and T are as in Fig. 1. $\Delta\mu_0$ is the deviation of μ at $B=0.0$ T. (b) The standard deviation of the electron density Δn_s as a function of B for $\Delta n_{s0}/\bar{n}_{s0}=0.01$ (solid line) and 0.03 (dashed line).

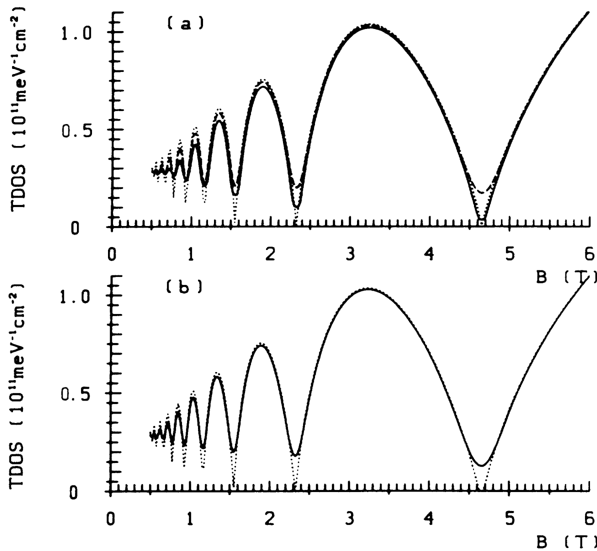

FIG. 6. (a) The effective TDOS for the n_s-Gaussian model with $\Delta n_s/\bar{n}_s=0.0$ (dotted line), 0.03 (dashed line), and for the μ-Gaussian model with $\Delta n_s/\bar{n}_s=0.05$ (solid line) vs magnetic field B. $\bar{n}_s=2.25\times10^{11}$ cm^{-2}, $T=1.64$ K, and $\Gamma=0.3\sqrt{B[T]}$ meV. (b) The TDOS for the n_{s0}-Gaussian model for $\Delta n_{s0}/\bar{n}_{s0}=0.0$ (dotted line) and 0.03 (solid line) vs B, $\bar{n}_{s0}=2.25\times10^{11}$ cm^{-2}, $N_A d=1.44\times10^{11}$ cm^{-2}, and T and Γ are as in (a).

would thus have constant n_s in an inhomogeneous sample. Fluctuations in acceptor and donor distributions would be unscreened. The presence of unscreened charges would lead to large potential fluctuation through the Poisson equation, implying large $\Delta\mu$ [cf. Eq. (2.7)] in contradiction to the initial assumption. Therefore, we assume for the μ-Gaussian distribution that Δn_s, not $\Delta\mu$, is independent of B. The choice of a constant Δn_s, independent of B, leads to a self-consistency relation between the effective LL width and the average TDOS at the Fermi level, yielding a finite TDOS between the LL's. It is interesting to note that this aspect is shared by recent theories of self-consistent screening of long-range scattering[14,15] where the screening of the impurities determines the level broadening and therefore the DOS, while the broadening itself depends on the DOS at the Fermi level. In the following calculations concerning the μ-Gaussian distribution we will not use the oversimplified approximation (3.7).

As is seen in Fig. 6(a) the μ-Gaussian model is not as efficient in creating a DOS between the LL's as the n_s-Gaussian model for corresponding Δn_s values. The qualitatively different properties of these models may be understood from the different mechanism involved in creating the DOS in between the LL's. The largest contribution to the "background" in the n_s-Gaussian model is drawn from the centers of the LL's [cf. Fig. 2(a)], while the μ-Gaussian model emphasizes the tails of the LL's. This difference is also the cause for the large effective linewidth of the μ-Gaussian model at low magnetic field B, where the tails of the LL's overlap significantly [cf. Fig. 3(c)]. The effective linewidth increases sharply, when an integer number of LL's is occupied. This effect is in accordance with results of self-consistent screening calculations[13,14] where, on the other hand, an oversimplified approximation leads to elliptically shaped LL's. So in contrast with our simple model these self-consistent screening theories do not give physically realistic results for the TDOS of overlapping LL's.

In a realistic statistical model one would not only expect $\Delta\mu$ to be a function of B as in the μ- and n_s-Gaussian model [cf. Figs. 2(b) and 3(b)] but also Δn_s would depend on B and the filling factor. The n_{s0}-Gaussian model has such properties, as is seen in Figs. 5(a) and 5(b), where in addition to $\Delta\mu$ becoming large at integer filling factors as in the other models, Δn_s also decreases in the same regions. This model is just slightly less effective in creating a background than the n_s-Gaussian model (cf. Fig. 6) due to the slight dips occurring in Δn_s in between LL's as is seen in Fig. 5(b), and the simultaneous reduction in the $\Delta\mu$ peaks in Fig. 5(a) as compared to the n_s-Gaussian model [cf. Fig. 2(b)]. It is also clear from Fig. 4(b) that the whole LL does contribute to the effective background in contrast to the other two models. As a result, the probability of the chemical potential being in between the LL's is neither vanishingly small as in the n_s-Gaussian model [cf. Fig. 2(a)] nor as great as in the μ-Gaussian model. The n_s distribution in this model seen in Fig. 4(a) [contrasted with the n_s distribution for the μ-Gaussian model in Fig. 3(a)] is very close to being Gaussian with a very sharp extremely high peak

superimposed where n_s as a function of n_{s0} develops a flat region, seen in Fig. 4(c) [cf. Eq. (3.1) with μ replaced by n_{s0}] with n_{s0} corresponding to an integer filling factor at the respective magnetic field B.

It is thus clear that these three statistical models do in many respects reflect qualitatively properties of more sophisticated microscopic models[13,14] and at the same time are not beset with the problems of unrealistic DOS.

IV. QUALITATIVE COMPARISON WITH EXPERIMENTS

The experiments for measuring the specific heat,[6] the capacitance,[1,2] the magnetization,[1] the gate current,[1] or the gate voltage[2] of a 2D EG in a heterostructure have all been carried out for different values of the electronic density n_s, the temperature, and the mobility. In most cases a simple parametric model of a Gaussian DOS superimposed on a constant background DOS has been used to interpret the experimental results. In order to present a coherent picture of the statistical model we have chosen one common set of parameters (cf. Sec. III) and will compare the results of the statistical model qualitatively with the simple background model and experimental results. We use Eq. (3.2) as the input DOS, which for the parameters chosen is vanishingly small between the LL's, so that the resulting apparent background DOS is clearly an effect of the inhomogeneities. In Figs. 7–9 the results are presented. The specific heat for the n_s-Gaussian model is shown in Fig. 7(a) and for the μ-Gaussian model in Fig. 8(a). It is evident that the 3%-n_s-Gaussian distribution ($\Delta n_s/\langle n_s\rangle=0.03$) creates much higher and smoother effective background in between the LL's than the 10%-simple background model, while the 5%-μ-Gaussian model creates about the same amount of background as that model. Away from the regions of integer filling factors the specific heat C_v of the statistical model coincides with the values given by the simple model with no background. This is due to the fact that in contrast with the simple background model the effective background in the statistical model is not created by taking away a fraction of the states from the initial Gaussian DOS in favor of a constant, magnetic-field-independent background. Compared to the experimental results[6] which are fitted reasonably well with a 20% background it can be seen that the n_s-Gaussian model would do the same for $\Delta n_s/\langle n_s\rangle$

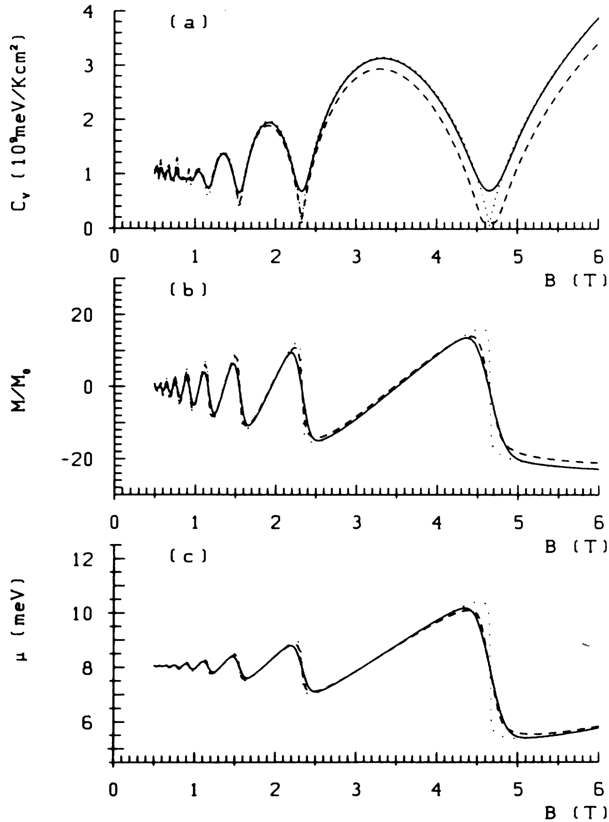

FIG. 7. (a) The specific heat, (b) magnetization, and (c) chemical potential of the n_s-Gaussian model for $\Delta n_s/\bar{n}_s=0.0$ (dotted line), 0.03 (solid line), and for $\Delta n_s/\bar{n}_s=0.0$ with a 10% background (dashed line) vs the magnetic field B. The parameters $\bar{n}_s$, T, and Γ are as in Fig. 6(a).

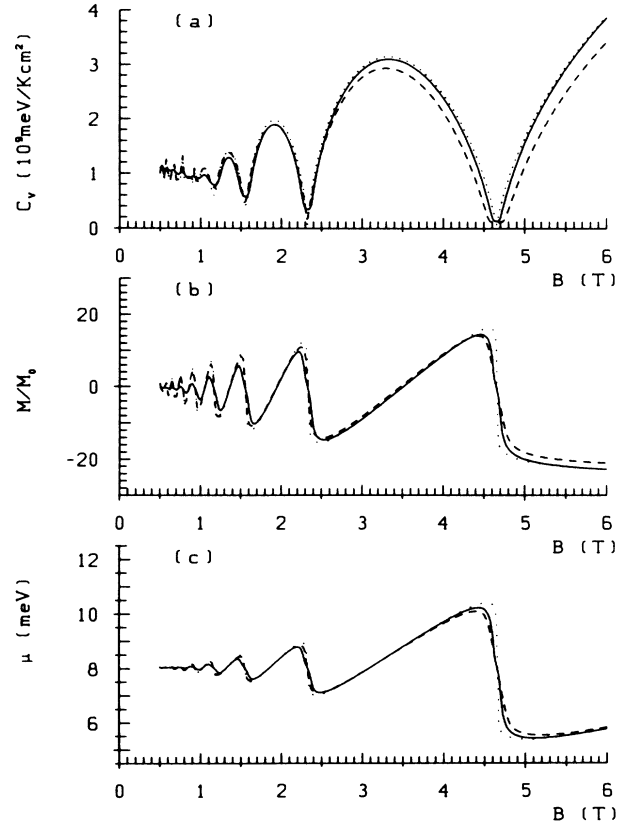

FIG. 8. (a) The specific heat, (b) magnetization, and (c) chemical potential of the μ-Gaussian model for $\Delta n_s/\bar{n}_s=0.0$ (dotted line), 0.05 (solid line), and for $\Delta n_s/\bar{n}_s=0.0$ with a 10% background (dashed line) vs the magnetic field B. The parameters $\bar{n}_s$, T, and Γ are as in Fig. 6(a). $M_0=2ekT/hc$.

$\sim 1-2\,\%$, while the μ-Gaussian model would not be able to recreate the low-B-field characteristics of C_v due to the large fluctuation of n_s needed to reproduce the effective background for large B. [This strongly depends though on the form chosen for $\Gamma(B)$.]

The capacitance measurements have been fitted both with a simple background model[1] and with a statistical model for low B.[1,2] In both cases a model assuming constant n_s is used instead of one in which the gate voltage V_g is fixed. This discrepancy has been pointed out,[1] but the simple n_s-constant model was used since the difference is small for the parameters of interest. But this difference becomes much more pronounced in the case when inhomogeneities of n_s are included. The minima in the capacitance C [cf. Fig. 9(a)] become much broader, comparable with the experimental results,[1] when the n_{s0}-Gaussian model is used. This is due to the fact that in this model n_s is variable as is seen in Fig. 9(c) and therefore the minima of C which occur for integer filling factors are not located at fixed B values during the averaging process.

The gate-current[1] measurement is probably most sensitive to the form of the DOS. If neither a simple background nor inhomogeneities are used in the n_{s0} model to fit the experimental results then the current peaks occurring at integer filling factor become too sharp and too high. If a simple background model is used [cf. Fig. 9(b)] the height of the peaks increases with increasing B as is seen in experiment until at higher B they become smaller with a flat top. This behavior contradicts the experimental results and may point to the artificiality of the flat B-independent background. On the other hand, the n_{s0}-statistical model reproduces the experimentally observed gradual increase of the current peaks with increasing B very well, see Fig. 9(b).

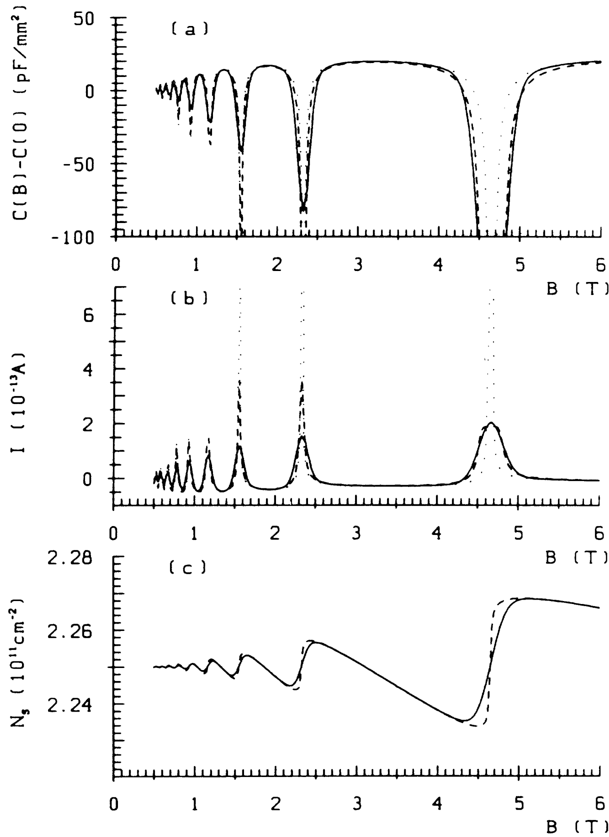

FIG. 9. (a) The differential capacitance, (b) the gate current, and (c) the electron density of the n_{s0}-Gaussian model for $\Delta n_{s0}/\bar{n}_{s0}=0.0$ (dotted line), 0.03 (solid line), and for $\Delta n_{s0}/\bar{n}_{s0}=0.0$ with a 10% background (dashed line) vs magnetic field B. The parameters $\bar{n}_{s0}$, $N_A d$, T, and Γ are as in Fig. 6(b). The thickness of the insulator is 845 Å. For the gate current in (b) we assume the sweep rate $dB/dT=1$ T/min and sample area 0.8 mm^2.

The magnetization measurement[7] has been fitted with extremely high LL broadening ($\Gamma=1.2$ meV) and no background. We have found that it may even better be fitted with lower broadening ($\Gamma=0.6$ meV) and very high background (40%), which points in the direction that the assumption of Gaussian shaped LL's may not be adequate in this case. It is therefore clear that in order to fit the statistical model to the experimental results, one would need a delicate balance between larger LL widths and rather high statistical fluctuations. This may indicate that in this multilayer sample the fluctuations are larger than believed.

In Figs. 7 and 8(c) it is seen that the μ-Gaussian and the n_s-Gaussian models can account for the smoothening effects as well as the simple background model. The gate voltage V_g between the gate and the 2D EG layer has been measured for a heterostructure as a function of B.[2] Such measurements seem to be extremely susceptible to external noise and inconclusive up until now. For a complete discussion we show though the chemical potential, which is proportional to V_g, in Figs. 7 and 8(c).

From the above discussion we have seen that the statistical model can explain most of the experimental results at least as well as the simple background model. In contrast to the latter it can explain physically the apparent DOS in between LL's. It has also been emphasized that the statistical model is a phenomenological model, and a microscopic approach is needed in order to derive more realistic distribution for n_s.

ACKNOWLEDGMENT

Stimulating discussions with K. von Klitzing are gratefully acknowledged.

APPENDIX: THE 2D EG IN EQUILIBRIUM WITH THE DEPLETION LAYER

Here the coupled Schrödinger and the Poisson's equations (2.1)—(2.4) will be considered for the boundary condition (2.6), i.e., the 2D EG is in equilibrium with the depletion layer. In the region $z>0$ (cf. Fig. 1) one obtains

$$V(z)=-\frac{4\pi e^2}{K_A}\left\{\frac{N_A d^2}{2}\left[1-2\frac{z}{d}+\left[\frac{z}{d}\right]^2\right]+n_s e^{-bz}\left[\frac{bz^2}{2}+2z+\frac{3}{b}\right]\right\}+(E_F+E_G-E_A)\,. \tag{A1}$$

Now one can use the fact that $1/b \ll d$ to neglect the term of the order $(z/d)^2$ when taking the expectation value of $V(z)$. Again we will arrive at the set of nonlinear equations (2.7)–(2.10) where the functional dependence of E_s and E_0 on n_s is now changed:

$$E_s = (E_F + E_G - E_A) - \frac{4\pi e^2}{K_A}\left[\frac{N_A d^2}{2} + \frac{3n_s}{b}\right], \quad \text{(A2)}$$

$$E_0 = \frac{\hbar^2 b^2}{8m} + (E_F + E_G - E_A) - \frac{4\pi e^2}{K_A}\left[\frac{N_A d^2}{2}\left[1 - \frac{6}{bd}\right] + \frac{15 n_s}{16 b}\right]. \quad \text{(A3)}$$

We solved this set of equations [(2.7)–(2.10) and (A2) and (A3)] with the condition that $V_g = \text{const}$, thus deriving n_s and $N_A d$ as functions of B. The result is shown in Fig. 10 where we can see that the variation of n_s is small, of the order of 1%, and that the variation of the depletion charge $N_A d$ is even smaller by an order of magnitude. Compared with Fig. 8(c) we therefore see that the variation of n_s is almost entirely due to changes in n_g, the gate charge. In the main text we therefore consider the model when $d \to \infty$ with $N_A d = \text{const}$. On the other hand, as mentioned before the $N_A d$ variation can be of importance in materials with short depletion length d (but still $d > 1/b$). In that case for example the capacitance becomes

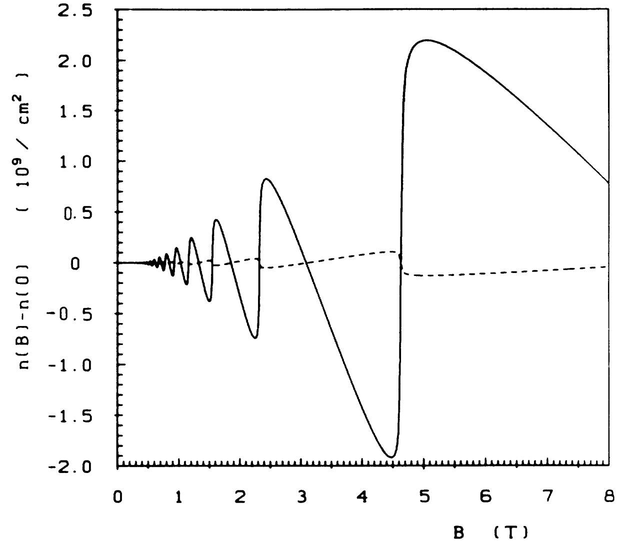

FIG. 10. The electron density $n_s(B) - n_s(0)$ (solid line) and the depletion charge density $N_A d(B) - N_A d(0)$ (dashed line) vs the magnetic field B, $n_s(0) = 2.25 \times 10^{11}$ cm^{-2}, $N_A d(0) = 1.44 \times 10^{11}$ cm^{-2}, and $N_A = 10^{15}$ cm^{-3}, and the parameters T and Γ are as in Fig. 6(b).

$$C = e\frac{dn_g}{dV_g} = \frac{D_T P + N_A(1 + D_T R)}{[D_T P + N_A(1 + D_T R)]/C_0 - [D_T P A + B(1 + D_T R)]/e^2}, \quad \text{(A4)}$$

where $C_0 = K_D / 4\pi L$ and

$$D_T = \frac{\partial n_s}{\partial \mu}, \quad \text{(A5)}$$

$$A = -\frac{4\pi e^2}{K_A}\frac{2}{b}\left[\frac{1 + \frac{48}{11}\frac{N_A d}{n_s}}{1 + \frac{32}{11}\frac{N_A d}{n_s}}\right], \quad \text{(A6)}$$

$$B = -\frac{4\pi e^2}{K_A} N_A d \left[1 - \frac{\frac{32}{11bd}}{\left[1 + \frac{32}{11}\frac{N_A d}{n_s}\right]}\right], \quad \text{(A7)}$$

$$P = -\frac{4\pi e^2}{K_A} N_A d \left[1 - \frac{4}{bd} - \frac{10}{11}\frac{1}{bd}\frac{\left[1 - \frac{16}{5}\frac{N_A d}{n_s}\right]}{\left[1 + \frac{32}{11}\frac{N_A d}{n_s}\right]}\right], \quad \text{(A8)}$$

$$R = -\frac{4\pi e^2}{K_A}\frac{19}{32b}\left[1 - \frac{10}{19}\frac{1}{bd}\frac{\left[1 - \frac{16}{5}\frac{N_A d}{n_s}\right]}{\left[1 + \frac{32}{11}\frac{N_A d}{n_s}\right]}\right]. \quad \text{(A9)}$$

This reduces to Eq. (2.13) for the case $d \to \infty$, $N_A d = \text{const}$. In the limit $N_A d \to 0$, $d \to \infty$, Eqs. (2.13) and (A4) have the same limiting form that has been used to fit the capacitance measurements.[1,2]

[1] D. Weiss, K. v. Klitzing, and V. Mosser, in *Two-Dimensional Systems: Physics and New Devices* Vol. 67 of *Springer Series in Solid-State Sciences,* edited by G. Bauer, F. Kuchar, and H. Heinrich (Springer, Berlin, 1986), p. 204.

[2] T. P. Smith, B. B. Goldberg, P. J. Stiles, and M. Heiblum, Phys. Rev. B **32**, 2696 (1985).

[3] B. Tausendfreund and K. von Klitzing, Surf. Sci. **142**, 220 (1984).

[4]D. Weiss, E. Stahl, G. Weimann, K. Ploog, and K. v. Klitzing, in Proceedings of the Sixth International Conference on Electronic Properties of Two-Dimensional Systems, Japan, 1985 (unpublished); J. Phys. C **18**, L783 (1985).

[5]M. G. Gavrilov and I. V. Kukushkin, Pis'ma Zh. Eksp. Teor. Fiz. **43**, 79 (1986) [JETP Lett. **43**, 103 (1986)].

[6]E. Gornik, R. Lassnig, G. Strasser, H. L. Störmer, A. C. Gossard, and W. Wiegmann, Phys. Rev. Lett. **54**, 1820 (1985).

[7]J. P. Eisenstein, H. L. Störmer, V. Narayanamurti, A. Y. Cho, A. C. Gossard, and C. W. Tu, Phys. Rev. Lett. **55**, 875 (1985).

[8]T. Ando and Y. Uemura, J. Phys. Soc. Jpn. **36**, 959 (1974); T. Ando, *ibid*. **37**, 622 (1974).

[9]R. R. Gerhardts, Z. Phys. B **21**, 275 (1975); **21**, 285 (1975); Surf. Sci. **58**, 234 (1976).

[10]F. Wegner, Z. Phys. B **51**, 279 (1983).

[11]A. Klein and J. F. Perez, Nucl. Phys. B **251**, 199 (1985).

[12]D. Heitmann, M. Ziesmann, and L. L. Chang, Phys. Rev. B **34**, 7463 (1986).

[13]R. Lassnig and E. Gornik, Solid State Commun. **47**, 959 (1983).

[14]T. Ando and Y. Murayama, J. Phys. Soc. Jpn. **54**, 1519 (1985).

[15]W. Cai and T. S. Ting, Phys. Rev. B **33**, 3967 (1986).

[16]R. T. Zeller, F. F. Fang, B. B. Goldberg, S. L. Wright, and P. J. Stiles, Phys. Rev. B **33**, 1529 (1986).

[17]R. R. Gerhardts and V. Gudmundsson, Phys. Rev. B **34**, 2999 (1986).

[18]F. F. Fang and W. E. Howard, Phys. Rev. Lett. **16**, 797 (1966).

[19]F. Stern, Phys. Rev. B **5**, 4891 (1972).

[20]D. Delagebeaudeuf and N. T. Linh, IEEE Trans. Electron Devices **29**, 955 (1982).

[21]T. Ando, J. Phys. Soc. Jpn. **51**, 3893 (1982).

[22]F. Stern, Appl. Phys. Lett. **43**, 974 (1983).

[23]F. Stern and S. Das Sarma, Phys. Rev. B **30**, 840 (1984).

[24]G. Bastard, Surf. Sci. **142**, 284 (1984).

[25]P. Gies and R. R. Gerhardts, Surf. Sci. **178**, 149 (1986).

[26]W. Zawadski and R. Lassnig, Surf. Sci. **142**, 225 (1984).